Stochastic Anomaly Simulation for Maxilla Completion from Cone-Beam Computed Tomography

Yixiao Guo[1 [0009−0002−5613−684X]], Yuru Pei✉[1 [0000−0001−8520−3509]], Si Chen[2 [0000−0003−4195−6351]], Zhi-bo Zhou[2 [0000−0001−5476−9921]], Tianmin Xu[2 [0000−0001−6975−6226]], and Hongbin Zha[1 [0000−0001−5860−4673]]

[1] School of Intelligence Science and Technology, Key Laboratory of Machine Perception (MOE), State Key Laboratory of General Artificial Intelligence, Peking University, Beijing 100871, China
peiyuru@cis.pku.edu.cn
[2] School of Stomatology, Peking University, Beijing, China

Abstract. Automated alveolar cleft defect restoration from cone beam computed tomography (CBCT) remains a challenging task, considering large morphological variations due to inter-subject abnormal maxilla development processes and a small cohort of clinical data. Existing works relied on rigid or deformable registration to borrow bony tissues from an unaffected side or a template for bony tissue filling. However, they lack harmony with the surrounding irregular maxilla structures and are limited when faced with bilateral defects. In this paper, we present a stochastic anomaly simulation algorithm for defected CBCT generation, combating limited clinical data and burdensome volumetric image annotation. By respecting the facial fusion process, the proposed anomaly simulation algorithm enables plausible data generation and relieves gaps from clinical data. We propose a weakly supervised volumetric inpainting framework for cleft defect restoration and maxilla completion, taking advantage of anomaly simulation-based data generation and the recent success of deep image inpainting techniques. Extensive experimental results demonstrate that our approach effectively restores defected CBCTs with performance gains over state-of-the-art methods.

Keywords: Deep volumetric inpainting · Maxilla completion · Stochastic anomaly simulation.

1 Introduction

Virtual maxilla completion from a cleft defected cone beam computed tomography (CBCT) plays an essential role in the noninvasive diagnosis and treatment planning of the secondary alveolar bone grafting procedure [7, 19]. Automatic cleft defect location and demarcation enable quantitative assessments of the cleft defect volume and grafting materials, relieving excessive or inadequate harvesting of grafting materials [1, 5, 8, 16]. Conventional methods relied on interactive free-form tracing tools [5, 17, 18], thresholding [9] and region-growing [9,

22]-based segmentation methods, to outline cleft defect boundaries from slices. However, manual annotation is tedious and highly dependent on practitioners' experiences. The segmentation techniques are limited in locating labial and palatal cortice boundaries with almost no textural variations due to soft tissue padding. Registration-based methods [11, 12, 15, 18] exploit shape priors from unaffected sides or normal templates for maxilla completions, though highly relying on template selection and semantic correspondence around defects.

With recent advances in deep neural networks, learning-based pixel-level image-inpainting models have gained great success. The deep inpainting models use the generative adversarial network (GAN) and autoregressive models to enforce the generative capacities for filling missing pixels [13, 20, 24, 25]. Random masking with a certain distribution makes it feasible to learn the inpainting model in an unsupervised manner, greatly relieving data collection burdens. However, when confronted with bony tissue restorations from defected volumetric CBCT images, we need to address two challenging issues. First, the cleft defects take on a large variety of morphologies due to inter-subject abnormal maxilla developments. The commonly used regular masks are limited to capturing the harmony of irregular cleft defects and surrounding maxilla for reasonable bony tissue filling. Unlike the protocol of image inpainting with a predefined binary mask for content prediction, there is no explicitly defined cleft defect mask for voxel prediction. In particular, automatic demarcation of cleft defects is desirable when given bony tissue restorations. Second, there is a lack of abundant clinical data for model learning, considering radiation hazards in volumetric image collection. Data augmentation with random transformations, such as image cropping and volumetric deformations, is feasible to combat data deficiencies. However, existing data augmentation is limited to accounting for the shape diversity of cleft defects and are suspicious in generalization capacities for bony tissue filling of clinical defected CBCTs.

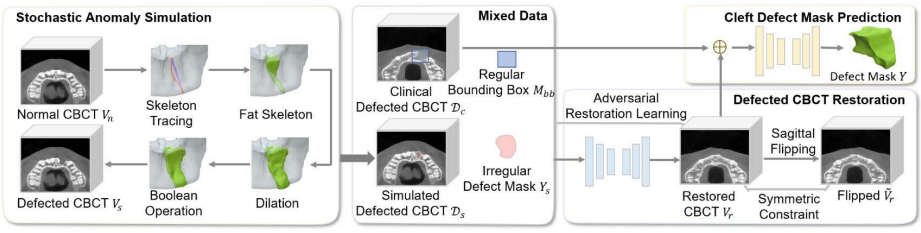

Fig. 1. Overview of the proposed stochastic anomaly simulation (SAS) for maxilla completion framework. The SAS algorithm relies on iterative skeleton tracing and dilation for diversified defected CBCT generation. The mixed clinical CBCT with regular bounding boxes and SAS-based generated data with irregular defect masks are used for adversarial learning of the restoration module. The cleft defect mask prediction module learned from the restored volumes enables cleft defect mask estimation.

In this paper, we propose a stochastic anomaly simulation (SAS) algorithm for defected CBCT generation, providing abundant simulated defected CBCT paired with cleft defect masks for learning the restoration model. The SAS algorithm respects the craniofacial fusion process guided by the Tessier system of orofacial clefting and simulates a cleft defect mask by iterative skeleton tracing and dilation, relieving gaps between the generated and clinical data. We present a weakly supervised volumetric image inpainting model for cleft defect restoration and maxilla completion, which is learned from clinical and SAS-based simulated data. Instead of existing image inpainting techniques dependent on random or predefined masks, the proposed model is capable of identifying the irregular boundary of cleft defects without requiring voxel-wise annotations. We further utilize adversarial restoration learning and craniofacial symmetry to encourage harmonic maxilla restoration. Qualitative and quantitative experiments on the clinical defected CBCTs demonstrate that the proposed method is effective in cleft defect restoration and maxilla completion, with performance gains over state-of-the-art methods. The main contributions of this work are as follows:

- We design a novel stochastic anomaly simulation algorithm for defected CBCT generation specific to abnormal maxilla developments, providing a new perspective on shape diversities regarding abnormal fusion of facial processes and greatly relieving the data collection and annotation burden.
- We present a volumetric inpainting framework with adversarial restoration learning and craniofacial symmetry for harmonic volumetric restoration of missing bony tissues.
- We have evaluated our approach on cleft defect restoration and maxilla completion on clinically obtained defected CBCTs. Experimental results demonstrate superior restorations compared with state-of-the-art methods.

2 Method

Fig. 1 shows the workflow of the proposed SAS-based data generation for cleft defect restoration and maxilla completion from CBCTs. Given a defected CBCT $V \in \mathbb{R}^n$ with n voxels, the goal is to infer restored volume $V_r \in \mathbb{R}^n$ with filled bony voxels in the cleft defect regions and binary cleft defect mask $Y \in \mathbb{R}^n$. To combat the limited clinical defected CBCTs and burdensome voxel-wise annotation, we propose the SAS algorithm for defected CBCT generation. Given a normal CBCT V_n with a complete maxilla, the SAS algorithm aims to generate the simulated defected CBCT V_s and the associated cleft defect mask Y_s by iterative skeleton tracing and dilation. We employ both clinical CBCT $\mathcal{D}_c$ and SAS-based simulated data $\mathcal{D}_s$ with irregular defect masks for model training. Instead of relying on predefined masks, the proposed defect restoration model is feasible to realize harmony between the filled bony tissues and the maxilla, by taking advantage of adversarial restoration learning and craniofacial symmetry. The cleft defect mask prediction module takes the defected CBCT and its restoration as input, which realizes an end-to-end inference of cleft defect masks.

2.1 Stochastic Anomaly Simulation

Confronted with a small cohort of defected CBCT scans in the clinical study, we present the SAS algorithm to simulate the inverse facial fusion process to generate defected CBCTs. Under the Tessier system of orofacial clefting, the alveolar cleft defect occurs in zones 1-2. To begin with, we conduct skeleton tracing in the bounding box of zones 1-2. Let s_u and s_l denote sampled points on the upper and lower bounding planes, respectively. Without loss of generality, we start skeleton tracing from s_l. In the i-th step, the skeleton growing vector q_i is defined using a randomly perturbed vector a and the vector towards s_u.

$$q_i = q_{i-1} + \mu_1 a + \mu_2 \left(\frac{\|s_{i-1} - s_u\|}{\|s_u - s_l\|} + \epsilon \right)^{-3} \cdot \frac{s_u - s_{i-1}}{\|s_u - s_{i-1}\|}, \tag{1}$$

where $a \sim \mathcal{N}(0, I)$. μ_1 and μ_2 are the perturbation strength parameters. The cleft skeleton becomes twisty with an increasing perturbation parameter of μ_1. ϵ is set to 1e-6. The skeleton point is updated as: $s_i = s_{i-1} + \frac{q_i}{\|q_i\|}$. Instead of using the single-voxel skeleton, voxels inside a cube centered at s are put into the fat skeleton s_{fat}. Considering the cleft defects tend to have increasing cross sections when they go from the upper dentition to the nasal plane, we define the side length r of the cube according to its height $\eta(s_i)$, and $r = \frac{\eta(s_i)}{\eta(s_u)} \cdot r_0$. r_0 denotes the predefined size. $\eta(s)$ denotes the perpendicular distance from the skeleton point s to the lower bounding plane. The skeleton tracing terminates when it reaches a predefined height or the upper bounding plane.

Given the fat skeleton s_{fat}, the cleft defect mask Y_s is generated using iterative dilation. Here we apply a set of 3D convolutional dilation filters to the fat skeleton κ times. κ is the dilation strength parameter. Finally, the volumetric intersection operator is applied to the maxilla mask Y_m and the cleft defect mask Y_s. The resultant cleft defect mask $Y_s = Y_s \otimes Y_m$. Fig. 2 shows sampled cleft defects generated using the SAS algorithm. Under the assumption that the cleft defect regions are padded with soft tissues, the simulated defected CBCT V_s is generated by setting voxel values inside the cleft defect to the average value of soft tissues perturbed by random noise.

2.2 Defected CBCT Restoration

The restoration model is initialized using the simulated data $\mathcal{D}_s$ with paired defected and normal CBCTs. The supervised reconstruction loss is defined using the l_1-norm regarding the restored volume V_r of the simulated defected CBCT V_s and the normal CBCT V_n, and $\mathcal{L}_{sup} = \sum_{(V_s, V_n) \in \mathcal{D}_s} \|V_n - V_r\|_1$. By minimizing $\mathcal{L}_{sup}$, the restored maxilla from the V_s is required to be consistent with the ground truth normal CBCT V_n.

Adversarial Restoration Learning from Clinical Data. The defected CBCT restoration model performs the voxel-to-voxel translation from the defected volume to the normal CBCT with the complete maxilla. In order to enforce consistency between the restored and normal CBCTs, we introduce adversarial

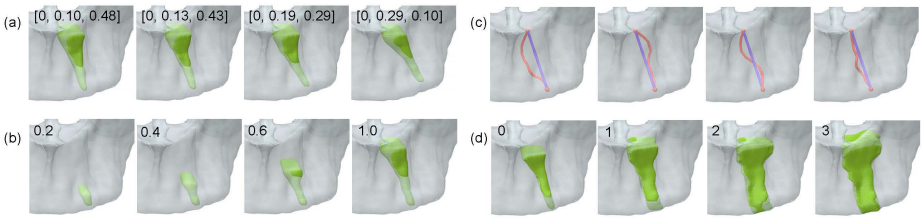

Fig. 2. Generated cleft defects with various values of (a) s_l, and (b) skeleton height. (c) Randomly generated skeletons (red), where the line between s_l and s_u is plotted in blue. (d) Generated cleft defects with different dilation strengths κ.

restoration learning for the cleft defect restoration and maxilla completion. Considering that the defected CBCT in the clinical dataset $\mathcal{D}_c$ has no annotations of the irregular cleft defects or the ground-truth restored volumes, the reconstruction loss is defined by the masked image similarity and Wasserstein GAN with gradient penalty (WGAN-GP) [2].

$$\mathcal{L}_{rec} = \sum_{V \in \mathcal{D}_c} \|\tilde{M} \odot (V - V_r)\|_1 - \beta \mathbb{E}_{V_r \in \mathcal{P}_r}[h(V_r)] + \mathcal{L}_{wgan}. \tag{2}$$

Under the observation that the regular bounding box comprises not only cleft defects but also residual bony tissues needed to be preserved, we define the residual bone mask M_{rb}. Since the region of the cleft defects is padded with soft tissues or air, the entry of M_{rb} is set to 1 when it belongs to the bony tissues in the bounding box and 0 otherwise by thresholding. Here we use a mixed mask $\tilde{M} = M_{rb} \oplus (1 - M_{bb})$ as the union of the regular bounding box mask M_{bb} and the residual bony mask M_{rb}. The WGAN-GP loss $\mathcal{L}_{wgan} = \mathbb{E}_{V_r \in \mathcal{P}_r}[h(V_r)] - \mathbb{E}_{V_n \in \mathcal{P}_n}[h(V_n)] + \lambda \mathbb{E}_{\hat{V} \in \hat{\mathcal{P}}_n}[\|\nabla_{\hat{V}} h(\hat{V}) \odot M_{bb}\|_2 - 1]^2$. The WGAN-GP loss is defined based on the Kantorovich-Rubinstein duality of the restored CBCT distribution $\mathcal{P}_r$ and the normal CBCT distribution $\mathcal{P}_n$. h denotes the 1-Lipschitz function. $\hat{V}$ is defined as a linear combination of samples $V_r \in \mathcal{P}_r$ and $V_n \in \mathcal{P}_n$, and $\hat{V} = \nu V_r + (1-\nu)V_n$, $\nu \in [0, 1]$. The element-wise product with the mask is used to constrain the gradient penalty inside the mask region to infer missing voxels.
Symmetric Constraint. Considering the symmetric characteristics of the maxilla, the restored CBCT V_r is required to satisfy the sagittal symmetric constraint. Since there is no annotation of the symmetric plane, we conduct the rigid alignments between V_r and its sagittally mirrored volume $\tilde{V}_r$. The symmetric regularization loss $\mathcal{L}_{sym} = \|V_r - g(\tilde{V}_r)\|_1$, where g denotes the rigid alignment operation.

The overall loss function is defined as a weighted combination of supervised reconstruction, adversarial restoration learning, and symmetric constraints.

$$\mathcal{L} = \mathcal{L}_{sup} + \gamma_1 \mathcal{L}_{rec} + \gamma_2 \mathcal{L}_{sym}. \tag{3}$$

The hyperparameters γ_1 and γ_2 trade off the adversarial volumetric restoration and the symmetric constraints.

Cleft Defect Mask Prediction. When given the restored CBCT V_r, the registration-based attribute transfer and volumetric Boolean operation can be used to estimate the cleft defect mask. However, they required additional volumetric operations in the online testing process. In contrast, we utilize a 3D U-Net [6] to model the mapping function $f : [V, V_r] \rightarrow Y$ for an end-to-end inference of cleft defect masks, which is learned from the simulated data $\mathcal{D}_s$ with ground truth cleft defect masks. Unlike the U-Net-based segmentation model, which infers defect masks from just defected CBCTs, our approach exploits the restored volume V_r for a virtual view of bony tissues regarding the cleft defects. In the online testing process, the input defected CBCT V and its restoration V_r are fed to the cleft defect mask prediction module for defect map inference.

3 Experiment

Dataset and Metrics. The proposed model is evaluated on the clinical defected CBCT dataset $\mathcal{D}_c$, consisting of 37 defected CBCTs, which is randomly split into 24, 3, and 10 for training, validation, and testing, respectively. The simulated dataset $\mathcal{D}_s$ consists of 1560 triplets of the simulated defected CBCTs, the normal CBCTs, and the cleft defect masks generated from 52 clinical CBCTs with complete maxillas using the SAS algorithm, where 90% are used for training and the remaining for testing. In experiments, the CBCTs are re-sampled to a resolution of $128 \times 128 \times 128$ with a voxel size of $1.56\ mm \times 1.56\ mm \times 1.56\ mm$. We analyze the virtual maxilla completion and cleft defect volume estimation using the Dice similarity coefficient (DSC), the average Hausdorff distance (AHD), and the mean squared deviation (MSD).

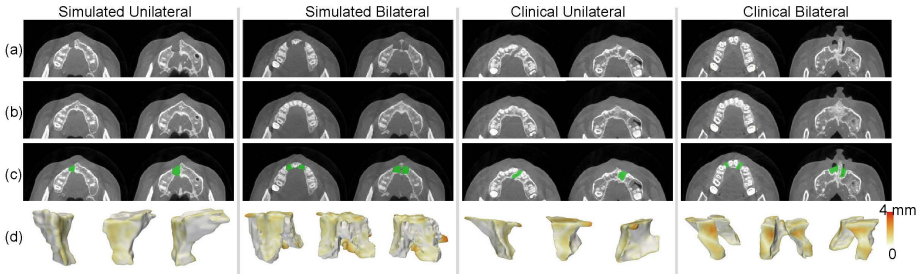

Fig. 3. Maxilla completion on simulated and clinical datasets with unilateral and bilateral cleft defects. (a) Input. (b) Restored CBCTs. (c) Estimated cleft defect masks. (d) Three views of estimated cleft defect surfaces with the MSD visualized.

Implementation Details. The proposed model is implemented on the inpainting model [10] using Pytorch toolkit, where the 2D convolutions are replaced by 3D convolutions to handle voxel-level inpainting. The perturbation parameters μ_1 and μ_2 in Eq. 1 are set to 0.15 and 0.05 respectively. The hyper-parameters

in $\mathcal{L}_{rec}$, $\mathcal{L}_{wgan}$, $\mathcal{L}$ are set as: $\beta = 5e-4$, $\lambda = 10$, $\gamma_1 = 1$, and $\gamma_2 = 5$. The ADAM optimization algorithm is used with a learning rate of 1e-4 and the momentums of 0.9 and 0.999. In the training process, we first use the simulated data $\mathcal{D}_s$ to initialize the restoration module and the cleft defect mask prediction module. Then, we refine the restoration module using adversarial learning and symmetrical constraints by minimizing $\mathcal{L}$. We evaluate the proposed model on a PC with an NVIDIA GeForce RTX 3090 GPU. The training and online inference take approximately 140 hours and 0.45 seconds, respectively.

Qualitative Assessment. Fig. 3 illustrates virtual maxilla completion and cleft defect volume estimation of defected CBCTs from simulated and clinical datasets. The proposed model is feasible to predict the missing bony tissues inside irregular cleft defects, bearing smooth transitions with surrounding residual bony tissues for reliable virtual maxilla completion and cleft defect volume estimation. Table 1 reports the cleft defect estimation accuracy with a DSC of 0.82 on clinical data and 0.89 on simulated data.

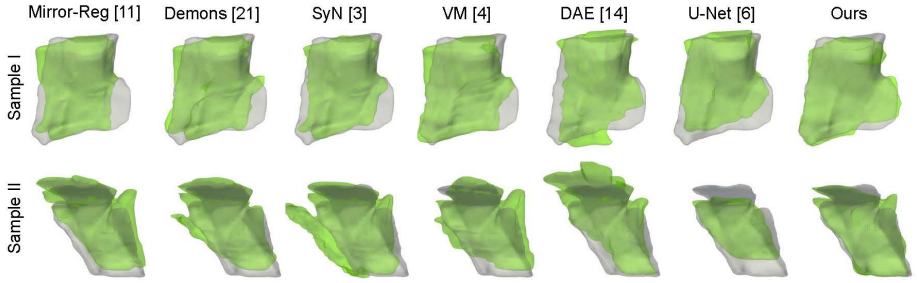

Fig. 4. Overlapping of the ground truth (gray) and estimated cleft defect surfaces (green) by compared methods.

Comparison. Table 1 and Fig. 4 report quantitative and qualitative results of cleft defect volume estimation by compared methods, including the rigid mirror registration [11], Demons [21], and SyN [3]-based registration. We also compare with the deep learning-based methods, including VM [4], DAE [14], U-Net [6], and the generative image inpainting (GII) [23] methods. As to the deep learning-based methods of VM, DAE, and GII, we use the same training and testing datasets as ours. We train the supervised U-Net-based segmentation model using paired defected CBCTs and cleft defect masks of $\mathcal{D}_s$. Our method outperforms the registration-based methods by 0.12 of Mirror, 0.05 of Demons, 0.06 of SyN, and 0.09 of VM regarding the DSC. Unlike the DAE, which relied on random noise-based structure restoration, we exploit the adversarial restoration learning to infer irregular cleft defect masks with performance gains of 0.10, 0.23 mm, and 0.30 mm in terms of the DSC, AHD, and MSD, respectively. The lack of textural variations in cranio-caudal and bucco-palatal boundaries makes it difficult to learn the segmentation model [6]. As to the deep inpainting GII [23],

we extend the inpainting model from 2D images to 3D defected CBCTs for voxel-level inference of missing bony tissues. The inpainting model is feasible to fill the masked region, though it does not address the morphological variations of irregular cleft defects. Instead, we exploit cleft defect simulation and adversarial restoration learning for voxel-wise tissue inference, outperforming GII by 0.05 and 0.10 regarding the DSC on the clinical and simulated datasets, respectively.

Table 1. Cleft defect estimation accuracies on clinical dataset $\mathcal{D}_c$ and simulated dataset $\mathcal{D}_s$. (SD-simulated data , AL-adversarial learning, and SC-symmetric constraint)

	$\mathcal{D}_c$			$\mathcal{D}_s$		
	DSC	AHD (mm)	MSD (mm)	DSC	AHD (mm)	MSD (mm)
Mirror [11]	0.70±0.18	0.71±1.07	1.25±1.19	0.77±0.17	0.55±0.64	0.90±0.71
Demons [21]	0.77±0.05	0.29±0.12	0.74±0.17	0.77±0.14	0.47±0.37	0.78±0.44
SyN [3]	0.76±0.08	0.32±0.24	0.79±0.30	0.79±0.13	0.44±0.40	0.73±0.44
VM [4]	0.73±0.07	0.38±0.15	0.84±0.22	0.72±0.10	0.63±0.29	1.10±0.36
DAE [14]	0.72±0.09	0.45±0.35	0.92±0.46	0.73±0.10	0.75±0.67	1.22±0.81
DAE_{SD} [14]	0.74±0.09	0.42±0.28	0.88±0.41	0.75±0.10	0.60±0.30	1.03±0.38
U-Net [6]	0.75±0.05	0.27±0.12	0.79±0.17	0.53±0.21	1.46±1.21	2.22±1.36
U-Net_{SD} [6]	0.80±0.05	0.23±0.08	0.67±0.11	0.88±0.08	0.16±0.15	0.43±0.24
GII [23]	0.77±0.05	0.33±0.15	0.78±0.22	0.79±0.09	0.42±0.26	0.84±0.34
w/o SD	0.80±0.05	0.26±0.13	0.67±0.22	0.75±0.09	0.52±0.23	0.99±0.29
w/o AL	0.81±0.05	0.26±0.10	0.66±0.16	0.87±0.06	0.19±0.12	0.51±0.22
w/o SC	0.80±0.07	0.24±0.12	0.63±0.23	0.88±0.07	0.19±0.18	0.49±0.32
Ours	**0.82±0.04**	**0.22±0.09**	**0.62±0.18**	**0.89±0.06**	**0.14±0.11**	**0.42±0.23**

Ablation Study. We have conducted an ablation study to validate the SAS-based simulated data (SD), adversarial restoration learning (AL), and the symmetric constraint (SC) as shown in Table 1. Results indicate that cleft defect-specific data augmentation with the SD and adversarial learning make it feasible to model shape distributions regarding inter-subject shape variations, enhancing the generalization capacity for cleft defect estimation. The SD also improves the DAE and U-Net with an AHD gap of 0.03 mm and 0.04 mm on $\mathcal{D}_c$. Moreover, the SC on the restored volumes has shown positive effects on both clinical and simulated datasets. Qualitative results on maxilla completion and defect mask prediction by variants are shown in the supplementary.

4 Conclusion

This paper has presented an anomaly simulation algorithm for diversified defected CBCT generation, respecting abnormal maxilla developments and relieving data collection burden. Given the SAS-based defected CBCT generation, we have exploited the volumetric inpainting with adversarial restoration learning and symmetric criteria, where the filled bony tissues are harmonic with the surrounding maxilla and facilitate cleft defect mask prediction. The proposed

approach takes advantage of both SAS-based defected CBCT generation and clinical data, which energizes end-to-end defected CBCT restoration and cleft defect mask estimation. Experimental results validate the proposed method on cleft defect volume prediction and maxilla completion.

The proposed SAS algorithm is specific to the 3D craniofacial fusion process involving the primary or secondary palate. The extension of the SAS algorithm to adapt to diversified abnormal developments of other diseases or organs deserves further study. Another limitation is that the proposed restoration model produces missing bony tissues conditioned on the input defected CBCTs. Considering patient-specific bone resorption after the grafting procedure, we would further investigate time-varying restoration learning in clinical applications.

Acknowledgments. This work was supported in part by National Natural Science Foundation of China under Grant 62272011, 61876008, and 82071172, Beijing Natural Science Foundation 7232337.

Disclosure of Interests. The authors have no competing interests to declare that are relevant to the content of this article.

References

1. Alonso, N., Tanikawa, D.Y.S., Freitas, R.d.S., Canan Jr, L., Ozawa, T.O., Rocha, D.L.: Evaluation of maxillary alveolar reconstruction using a resorbable collagen sponge with recombinant human bone morphogenetic protein-2 in cleft lip and palate patients. Tissue Engineering Part C: Methods **16**(5), 1183–1189 (2010)
2. Arjovsky, M., Chintala, S., Bottou, L.: Wasserstein gan. ArXiv **abs/1701.07875** (2017)
3. Avants, B., Epstein, Clgrossman, M., Gee, J.: Symmetric diffeomorphic image registration with cross-correlation: evaluating automated labeling of elderly and neurodegenerative brain. Medical Image Analysis **12**(1), 26–41 (2008)
4. Balakrishnan, G., Zhao, A., Sabuncu, M.R., Guttag, J., Dalca, A.V.: An unsupervised learning model for deformable medical image registration. In: IEEE conference on computer vision and pattern recognition. pp. 9252–9260 (2018)
5. Canan Jr, L.W., da Silva Freitas, R., Alonso, N., Tanikawa, D.Y.S., Rocha, D.L., Coelho, J.C.U.: Human bone morphogenetic protein-2 use for maxillary reconstruction in cleft lip and palate patients. Journal of Craniofacial Surgery **23**(6), 1627–1633 (2012)
6. Çiçek, Ö., Abdulkadir, A., Lienkamp, S.S., Brox, T., Ronneberger, O.: 3d u-net: learning dense volumetric segmentation from sparse annotation. In: International conference on medical image computing and computer-assisted intervention. pp. 424–432. Springer (2016)
7. De Mulder, D., Cadenas de Llano-Pérula, M., Jacobs, R., Verdonck, A., Willems, G.: Three-dimensional radiological evaluation of secondary alveolar bone grafting in cleft lip and palate patients: a systematic review. Dentomaxillofacial Radiology **48**(1), 20180047 (2019)
8. Dickinson, B.P., Ashley, R.K., Wasson, K.L., OąŕHara, C., Gabbay, J., Heller, J.B., Bradley, J.P.: Reduced morbidity and improved healing with bone morphogenic protein-2 in older patients with alveolar cleft defects. Plastic and Reconstructive Surgery **121**(1), 209–217 (2008)

9. Feng, B., Jiang, M., Xu, X., Li, J.: A new method of volumetric assessment of alveolar bone grafting for cleft patients using cone beam computed tomography. Oral surgery, oral medicine, oral pathology and oral radiology **124**(2), e171–e182 (2017)
10. Iizuka, S., Simo-Serra, E., Ishikawa, H.: Globally and locally consistent image completion. ACM Transactions on Graphics (TOG) **36**, 1 – 14 (2017)
11. Janssen, N.G., Schreurs, R., Bittermann, G.K., Borstlap, W.A., Koole, R., Meijer, G.J., Maal, T.J.: A novel semi-automatic segmentation protocol for volumetric assessment of alveolar cleft grafting procedures. Journal of Cranio-Maxillofacial Surgery **45**(5), 685–689 (2017)
12. Linderup, B.W., Küseler, A., Jensen, J., Cattaneo, P.M.: A novel semiautomatic technique for volumetric assessment of the alveolar bone defect using cone beam computed tomography. The Cleft Palate-Craniofacial Journal **52**(3), 47–55 (2015)
13. Liu, H., Jiang, B., Song, Y., Huang, W., Yang, C.: Rethinking image inpainting via a mutual encoder-decoder with feature equalizations. In: European Conference on Computer Vision (2020)
14. Morais, A., Egger, J., Alves, V.: Automated computer-aided design of cranial implants using a deep volumetric convolutional denoising autoencoder. In: World Conference on Information Systems and Technologies. pp. 151–160. Springer (2019)
15. Nagashima, H., Sakamoto, Y., Ogata, H., Miyamoto, J., Yazawa, M., Kishi, K.: Evaluation of bone volume after secondary bone grafting in unilateral alveolar cleft using computer-aided engineering. The Cleft Palate-Craniofacial Journal **51**(6), 665–668 (2014)
16. Ozawa, T., Omura, S., Fukuyama, E., Matsui, Y., Torikai, K., Fujita, K.: Factors influencing secondary alveolar bone grafting in cleft lip and palate patients: prospective analysis using ct image analyzer. The Cleft palate-craniofacial journal **44**(3), 286–291 (2007)
17. Shawky, H., Seifeldin, S.A.: Does platelet-rich fibrin enhance bone quality and quantity of alveolar cleft reconstruction? The Cleft palate-craniofacial journal **53**(5), 597–606 (2016)
18. Shirota, T., Kurabayashi, H., Ogura, H., Seki, K., Maki, K., Shintani, S.: Analysis of bone volume using computer simulation system for secondary bone graft in alveolar cleft. International journal of oral and maxillofacial surgery **39**(9), 904–908 (2010)
19. Stasiak, M., Wojtaszek-Słomińska, A., Racka-Pilszak, B.: Current methods for secondary alveolar bone grafting assessment in cleft lip and palate patientsąła systematic review. Journal of Cranio-Maxillofacial Surgery (2019)
20. Suvorov, R., Logacheva, E., Mashikhin, A., Remizova, A., Ashukha, A., Silvestrov, A., Kong, N., Goka, H., Park, K., Lempitsky, V.S.: Resolution-robust large mask inpainting with fourier convolutions. IEEE Winter Conference on Applications of Computer Vision (WACV) pp. 3172–3182 (2021)
21. Thirion, J.P.: Image matching as a diffusion process: an analogy with maxwell's demons. Medical image analysis **2 3**, 243–60 (1998)
22. Xi, T., Schreurs, R., Heerink, W.J., Berge, S.J., Maal, T.J.: A novel region-growing based semi-automatic segmentation protocol for three-dimensional condylar reconstruction using cone beam computed tomography (cbct). PloS one **9**(11), e111126 (2014)
23. Yu, J., Lin, Z.L., Yang, J., Shen, X., Lu, X., Huang, T.: Generative image inpainting with contextual attention. IEEE Conference on Computer Vision and Pattern Recognition pp. 5505–5514 (2018)

24. Yu, J., Lin, Z.L., Yang, J., Shen, X., Lu, X., Huang, T.S.: Free-form image inpainting with gated convolution. 2019 IEEE/CVF International Conference on Computer Vision (ICCV) pp. 4470–4479 (2018)
25. Zeng, Y., Fu, J., Chao, H., Guo, B.: Aggregated contextual transformations for high-resolution image inpainting. IEEE transactions on visualization and computer graphics (2021)